RADIATION CLIMATE MAP FOR ANALYZING RISKS TO ASTRONAUTS ON THE MARS SURFACE FROM GALACTIC COSMIC RAYS

Premkumar B. Saganti[1-2], Francis A. Cucinotta[2],
John W. Wilson[3], Lisa C. Simonsen[3], and *Cary Zeitlin[4]*

[1]Lockheed Martin Space Operations, Houston TX-77058;
[2]NASA Johnson Space Center, Houston, TX-77058;
[3]NASA Langley Research Center, Hampton, VA-23681
[4]Lawrence Berkeley National Laboratory, University of California, Berkeley, CA 94720

ABSTRACT

The potential risks for late effects including cancer, cataracts, and neurological disorders due to exposures to the galactic cosmic rays (GCR) is a large concern for the human exploration of Mars. Physical models are needed to project the radiation exposures to be received by astronauts in transit to Mars and on the Mars surface including the understanding of the modification of the GCR by the Martian atmosphere and identifying shielding optimization approaches. The Mars Global Surveyor mission has been collecting Martian surface topographical data with the Mars Orbiter Laser Altimeter (MOLA). Here we present calculations of radiation climate maps of the surface of Mars using the MOLA data, the radiation transport model HZETRN (high Z=atomic number and high energy transport), and the heavy ion fragmentation model QMSFRG. Organ doses and average number of particle hits per cell nucleus from GCR components (protons, heavy ions, and neutrons) are evaluated as a function of the altitude on the Martian surface. Approaches to improve the accuracy of the radiation climate map presented here using data from the Odyssey mission are discussed.

INTRODUCTION

The potential for harmful late effects including as cancer, cataracts, neurological disorders, and non-cancer mortality risks galactic cosmic rays (GCR) pose a major threat for the human exploration of Mars [1-3]. Because of their high energies, the GCR are extremely penetrating and cannot be eliminated by practical amounts of shielding [4, 5]. The high charge and energy HZE ions portion the GCR present unique challenges to biological systems such as DNA, cells, and tissue and the risks to humans is highly uncertain at this time [2, 5]. Another threat in deep space is solar particle events, which could induce acute radiation syndromes including death if the event is large enough. However, shielding by the Mars atmosphere and spacecraft structures along with early warning and detection systems may be effective as mitigation measures and the biological effects of protons are well understood being similar to gamma rays. Safety assurances and dose limits for the human exploration of Mars cannot be provided at this time due to the uncertainties in the biological effects of HZE ions [2]. Important physical data on the GCR isotopic and energy spectrum composition near Mars and on the Mars surface will be needed prior to human exploration. Developing methods for the accurate prediction of the modulation of the isotopic composition and energies of the GCR after nuclear and atomic interactions with Mars atmosphere and soil and the accurate determination of secondary neutron spectra will be essential to design and undertake such missions.

Robotic precursor missions to Mars can provide valuable data on the radiation environment to be encountered in future human exploration missions of the red planet and validation of models used for mission design. These measurements should include direct physical measurements with radiation spectrometers of the energy spectra of protons, heavy ions, and neutrons. Physical data related to the Mars altitude, atmospheric [6] and soil composition will also be valuable in developing models of astronauts and equipment exposures, and in designing shielding habitat

configurations. In this paper, we discuss the use of the MOLA altitude data [6] and models of the radiation environment and GCR transport to present the first complete radiation map of the Mars surface.

METHODS

The HZETRN transport code [4, 7] describes the atomic and nuclear reaction processes that alter the GCR in their passage through materials such as the Mars atmosphere and tissue. The HZETRN code solves the Boltzmann equation for the particle flux, $\phi_j(x,E)$, of ion of type j, with energy E, and depth x, is obtained from

$$\Omega \cdot \nabla \phi_j(x,\Omega,E) = \sum_k \int \sigma_{jk}(\Omega,\Omega',E,E')\phi_k(x,\Omega',E')dE'd\Omega' - \sigma_j(E)\phi_j(x,\Omega,E)$$

where σ_j is the total reaction cross section and σ_{jk} is the channel changing cross sections. The HZETRN code solves the Botzmann equation using the continuos slowing down approximation. The straight-ahead approximation is used for projectile nuclei [3] and angular dependence of scattering considered for neutrons [7]. Details on the numerical methods uses in transport code can be found in refs. [4, 7]. Nuclear fragmentation cross sections are described by the quantum multiple scattering (QMSFRG) model [8, 9]. The QMSFRG model considers the energy dependence of the nucleus-nucleus interaction, quantum effects in nuclear abrasion, and a stochastic model of the de-excitation of pre-fragment nuclei produced in projectile-target nuclei interactions. The organ dose equivalent can be found by integrating the particle energy spectra folded with the energy, mass, and charge dependent stopping power or linear energy transfer (LET), $L(E)$, and the LET dependent quality factor, $Q(L)$, and by considering the distribution of shielding at the tissue,

$$H_T = \Sigma_j \int dE\ \phi_j(x,E)\, L(E)\, Q[L(E)]$$

The organ dose equivalent is expressed in the units of Sievert (Sv) (1 cSv = 1 rem). Values of the LET dependent Q vary between 1 and 30 for the GCR with the highest values for LET = 50-200 keV/μm in the range of GCR ions with charge, Z=14-26.

The modulation of the GCR near Earth is described using the Badhwar et al. [10, 11] model in terms of the magnetic field deceleration parameter, Φ. GCR spectra for several solar maximum (Φ= 1060 or 1216 MV) and solar minimum (Φ = 428 MV) scenarios were generated. Differences in solar modulation and GCR composition near-Earth and near-Mars have not been considered in the calculations. The number of particle-hits per cell nucleus due to direct particle traversals [12] are evaluated using an average cell cross-sectional area of 100 μm^2. Calculations that include indirect cell hits from delta-rays (secondary electrons) produced by ions will be reported elsewhere. In some comparisons, heavy ions are divided into distinct charge groups in some calculations defined as Z=3-10 (light), Z=11-20 (medium), and Z=20-28 (heavy).

Low- and high-density Mars atmospheric models [13] (16 and 22 g/cm^2) assuming a spherically distributed CO_2 atmosphere are considered. Figure 1 describes the geometry used in the calculations. The resultant shielding offered by the CO_2 atmosphere at a given altitude location is calculated for a set of geodesic distributed rays using the relation

$$s(z,\theta) = \sqrt{(R+h)^2 \cos^2(\theta) + \left[2R(z-h) + z^2 - h^2\right]} - (R+h)\cos(\theta)$$

where, h is the altitude above the mean surface, s being the distance along the slant path with zenith angle, θ (is calculated between 0 and 90^0 with 1^0 increments) and z is the vertical length of the atmosphere above the identified location. Radiation transport along the rays are then evaluated using the HZETRN code and results integrated over z and h to obtain information at each location on the Martian surface.

Calculations of radiation transport in the human body, which locate astronauts at specific surface locations on Mars were performed using the methods described in conjunction with computerized anatomical models [14] to represent the self-shielding of the human body. Particle energy spectra, organ dose equivalent, and cell hits were evaluated at 12 representative different anatomical locations for solar minimum and solar maximum. Visualization of the Martian surface data was accomplished using the computer routines (VIZ-MARS) that we have developed for this application using the software package *MATLAB*.

RESULTS AND DISCUSSION

By combining the organ dose equivalent with age and gender specific risk coefficients an estimate of the probability of fatal cancer from radiation exposure is made [2, 5]. However, due to the limitations in radiobiological data and knowledge for HZE ions, the definition of a "dose equivalent" is highly uncertain [2, 5]. Thus estimating the expected risk from radiation fields in deep space and on the Mars surface relies on accurate evaluation the physical radiation fields as reported here, however awaits new radiobiology knowledge to define the resulting health risks to astronauts and to fully understand the effectiveness of risk mitigation approaches such as shielding. Estimates of cell damage [15, 16] have been considered along with the current organ dose equivalent to illustrate the role of attenuation of heavy ions by shielding such as the Martian atmosphere and spacecraft and tissue shielding.

The major physical processes that modulate the heavy ions are atomic energy loss processes that are well described by stopping powers, and nuclear reactions including fragmentation and production processes [4, 8, 17]. Figure 2a shows calculations of the probability that a GCR ion will suffer a nuclear collision per cm of path-length in water. Figure 2b shows the elemental distribution of the GCR and calculations of the number of nuclear reactions made by each GCR charge group per path-length in

water. These results illustrate the large number of interactions of the GCR that will occur with both tissue and the Mars atmosphere. However, the level of shielding provided is insufficient to completely eliminate the heavy ion components and an accurate description of both fragmentation and transport is needed. In Figure 3 we show results for the number of particle hits per cell as a function of altitude on the Mars surface for distinct charge groups and at solar minimum and solar maximum. The number of cell hits by light ions such as protons and helium are only modestly affected by atmospheric shielding (altitude variations). This is due to the balance of losses from atomic slowing down processes and gains from the fragmentation of heavy ions or production on atoms in the atmosphere. In contrast, heavy ions undergo a large reduction with increasing atmosphere (decreasing altitude), however the present models predict that an important heavy ion component occurs, especially at higher altitudes. Neutrons (not shown here) are less sensitive to changes in the amount of atmosphere since they contain an important back-scattered component at lower energies (< 100 MeV) [7]. Because neutrons will make up a larger contribution at low altitudes and production cross sections for neutrons are sensitive to target mass, information on atmospheric and soil composition will be important for designing surface habitats for astronauts. The Odyssey spacecraft [18] and future Lander missions should provide such data. Figure 4 and Figure 5 show results for the Martian radiation climate over the surface of Mars for protons and heavy ions, respectively at solar minimum and maximum. These results indicate significant reduction for heavy and medium ions, moderate reduction for light ions, and little or no reduction for protons and neutrons (neutrons not shown). Because of the large uncertainties in the biological effects of heavy ions and validation of these results by measurements on the surface of Mars will be essential for human safety.

Table 1 compares the organ dose equivalent en-route to Mars and on the Mars surface for the major tissues susceptible to radiation-induce cancers. Included in these calculations are results that consider the addition of shielding configurations on 5 or

10 cm of water equivalent material. The cruise phase of the mission leads to organ doses that approach or exceed legal exposure limits used in low Earth orbit [19] if time is not constrained and are currently deemed unacceptable because of the uncertainties in the risks from such an exposure [1, 3]. The comparison in Table 1 show that maximizing crew times on the Mars surface (conjunction class missions) will be favorable for human exploration. In Figure 6 we show a climatic map of the skin dose equivalent for the entire surface of Mars. Variations on the order or 50% are predicted due to changes in atmosphere. Although, uncertainties in heavy ion radiobiology including the radiation quality factors are expected to be much larger at this time than estimates of physical quantities, a validation of the radiation climate map described here is needed. Surface validation measurements should include measurements of LET spectra and the integral dose and dose equivalent [20] along with spectroscopic data on neutrons.

CONCLUSIONS

Calculations of the Martian radiation climate illustrate the level of detail that is now available by state-or-the art computer codes developed by NASA. Critical questions to be addressed include what is the current accuracy of these calculations, what accuracy will be required, and what measurements are needed to validate models? Previous comparisons with measurements near Earth provide some validation of the models use here and agreement to within 25% is found for the dose equivalent. However, clearly data near Mars and most importantly on the surface of Mars will be needed in light of the high level of concern of biological risks to astronauts from heavy ions. In the very near future, 2001 Mars Odyssey will be collecting the first Martian radiation environment data by the Martian Radiation Environment Experiment (MARIE) detector [20]. Other spacecraft that will land on Mars will provide other data. These measurements will then be utilized to verify our calculated

predictions and update the models as needed. Data on the Martian altitude and topology, and atmospheric and soil composition will also be valuable for designing human exploration missions.

REFERENCES

1. National Academy of Sciences Space Science Board, HZE Particle Effects in Manned Space Flight, National Academy of Sciences U.S.A. Washington D.C., 1973.

2. National Academy of Sciences, NAS. National Academy of Sciences Space Science Board, Report of the Task Group on the Biological Effects of Space Radiation. Radiation Hazards to Crews on Interplanetary Mission National Academy of Sciences, Washington, D.C., 1997.

3. Cucinotta, F.A., Manuel, F.K., Jones, J., Izsard, G., Murray, J., Djojenegoro, and Wear, M., Space Radiation and Cataracts in Astronauts. *Radiat. Res.* **156**, 460-466 2001.

4. Wilson J.W., Townsend, L.W., Schimmerling, W., Khandelwal G.S., Khan, F., Nealy, J.E., Cucinotta, F.A., Simonsen, L.C., and Norbury, J.W., Transport methods and interactions for space radiations, RP1257, NASA, Washington D.C., 1991.

5. Cucinotta, F.A., Schimmerling, W., Wilson, J.W., Peterson, L.E., Badhwar, G.D., Saganti, P., and Dicello, J.F., Space Radiation Cancer Risks and Uncertainties for Mars Missions. *Radiat. Res.* **156**, 682-688, 2001.

6. Smith, D.E., Zuber, M.T., Solomon, S.C., Philips, R.J., Head, J.W., Garvin, J.B., et al., The Global Topography of Mars and Implications for Surface Evolution. *Science* **284**, 1495-1503, 1999.

7. Clowdsley, M.S., Wilson, J.W., Kim, M., Singleterry, R.C., Tripathi, R.K., Heinbockel, J.H., Badavi, F.F., and Shinn, J.L., Neutron Environments on the Martian Surface. *Physica Medica* **17**, 94-96, 2001.

8. Cucinotta, F.A., Wilson, J.W., Tripathi, R.K.; and Townsend, L.W., Microscopic, Fragmentation Model For Galactic Cosmic Ray Studies. *Adv. in Space Res.* **22**, 533-537, 1998.

9. Cucinotta, F.A., Wilson, J.W., Shinn, J.L., Tripathi, R.K., Maung, K.M., Badavi, F.F., Katz, R., and Dubey, R.D.: Computational Procedures and Data-Base Development. In: NASA Workshop on Shielding Strategies for Human Space

Exploration. Eds. Wilson, J.W., Miller, J., Konradi, A., and Cucinotta, F.A., NASA CP 3360, 1997.

10. Badhwar, G.D., and O'Neill, P.M., An Improved Model of GCR for Space Exploration Missions. *Nucl. Tracks Radiat. Meas*. **20**, 403-410, 1992.

11. Badhwar, G. D., Cucinotta, F. A., and O'Neill, P. M.: An Analysis of Interplanetary Space Radiation Exposure for Various Solar Cycles. *Radiat. Res.* **138**, 201-208, 1994.

12. Cucinotta F.A., Nikjoo H., and Goodhead D.T., The Effects of Delta Rays on The Number of Particle-Track Traversals per Cell in Laboratory and Space Exposures. *Radiat. Res.* **150**, 115-119, 1998.

13. Simonsen, L.C., Wilson, J.W., Kim, M.H., and Cucinotta, F.A., Radiation Exposure for Human Mars Exploration. *Health Phys*. **79**, 515-525, 2000.

14. Billings, M.P., Yucker, W.R., and Heckman, B.R., Body Self-Shielding Data Analysis, McDonald Douglas Astronautics Company West, MDC-G4131, 1973.

15. Cucinotta, F.A., Wilson, J.W., Katz, R., Atwell, W., and Badhwar, G. D., Track Structure and Radiation Transport Models for Space Radiobiology Studies. *Adv. in Space Res.* **18**, 183, 194-203, 1995.

16. Cucinotta, F.A., and Dicello, J.F., On the Development of Biophysical Models for Space Radiation Risk Assessment. *Adv. Space. Res.* **25**, 2131-2140, 2000.

17. Zeitlin, C., Heilbronn, L., Miller, J., Rademacher, S.E., Borak, T., Carter, T.R., Frankel, K.A., Schimmerling, W., and Stronach, C.E., Heavy Fragment Production Cross Sections for 1.05 GeV/nucleon ^{56}Fe in C, AL, Cu, Pb, and CH_2 Targets. *Phys. Rev. C* **56**, 388-397, 1997.

18. References this special issue.

19. National Council on Radiation Protection and Measurements, Radiation Protection Guidance for Activities in Low Earth Orbit, NCRP Report 132, Bethesda MD , 2000.

20. Badhwar, G., this special issue.

Table-1: Illustration of the effectiveness from water shield (5 g/cm^2 and 10 g/cm^2) on the organ dose equivalent at 12 different locations in the human body. The top table are calculations during transit time to Mars and bottom table on shows the calculations on the Martian surface.

En-route to Mars	**Water Shield (g/cm^2) and corresponding Total Dose (cSv/yr)**				
				% Reduction with	
	0 g/cm^2	**5 g/cm^2**	**10 g/cm^2**	**5 g/cm^2**	**10 g/cm^2**
BFO	70.01	58.18	50.68	16.89	27.60
BLADDER	60.08	51.98	46.65	13.48	22.35
COLON	69.04	57.70	50.47	16.43	26.91
ESOPHAGUS	65.90	55.61	48.96	15.61	25.70
EYE	96.01	73.74	60.50	23.19	36.98
GONADS	73.71	60.03	51.68	18.56	29.89
LIVER	63.53	54.13	48.04	14.80	24.38
LUNG	66.82	56.22	49.39	15.86	26.08
POINT	120.02	95.61	74.26	20.34	38.13
SKIN	94.13	73.15	60.03	22.29	36.23
STOMACH	60.99	52.62	47.12	13.73	22.74
THYROID	72.57	59.82	51.75	17.58	28.69

On Mars Surface	**Water Shield (g/cm^2) and corresponding Total Dose (cSv/yr)**				
				% Reduction with	
	0 g/cm^2	**5 g/cm^2**	**10 g/cm^2**	**5 g/cm^2**	**10 g/cm^2**
BFO	19.41	18.66	18.08	3.86	6.86
BLADDER	21.09	19.73	18.88	6.43	10.47
COLON	19.19	18.50	17.95	3.63	6.48
ESOPHAGUS	19.05	18.40	17.88	3.43	6.16
EYE	19.68	18.82	18.17	4.41	7.68
GONADS	19.77	18.93	18.29	4.26	7.49
LIVER	19.59	18.79	18.18	4.08	7.21
LUNG	19.58	18.80	18.20	3.99	7.06
POINT	25.75	21.27	20.06	17.40	22.09
SKIN	19.33	18.60	18.02	3.81	6.78
STOMACH	21.12	19.83	18.97	6.10	10.18
THYROID	18.97	18.33	17.81	3.37	6.07

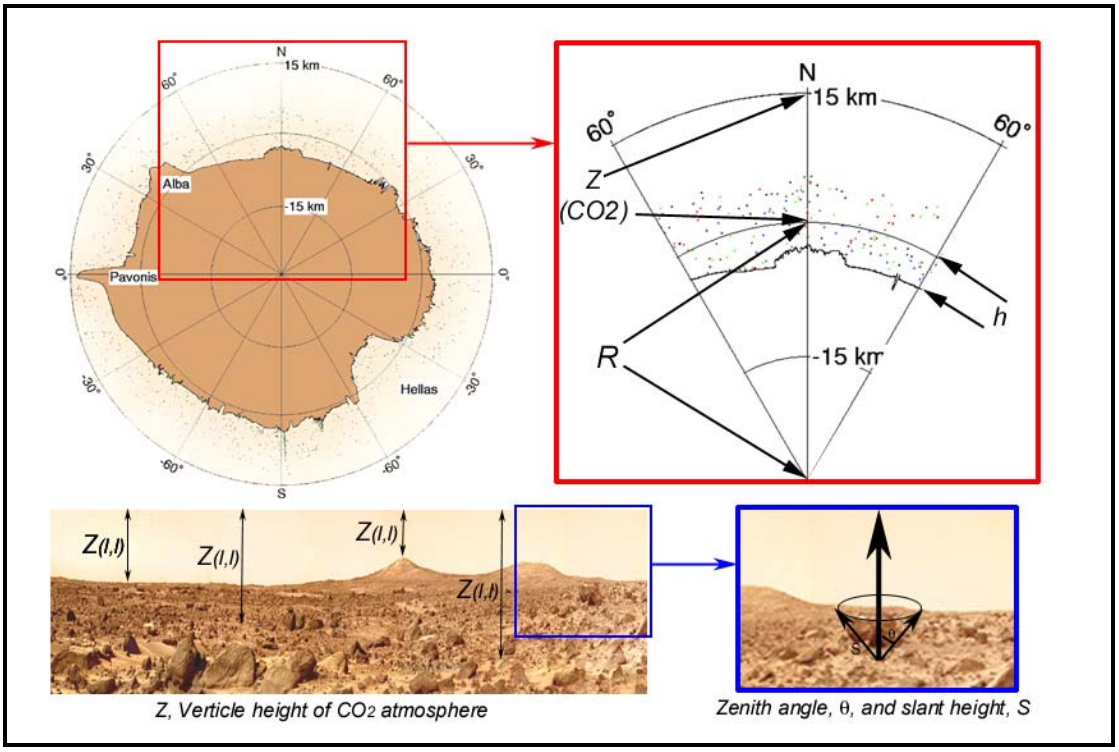

Figure-1. Top left image is an illustration of the global profile of the Martian surface from data obtained by MOLA crossing longitudes 52°E and 247°E. The north and south polar caps are at the top and bottom with a vertical exaggeration of 100:1 (adopted from Smith et al. [6]). Top right is the description of the mean surface radius, R, vertical height, Z, of the CO_2 atmosphere above the mean surface, and height of the target point above / below the mean surface as used in the calculations. Bottom left is the Martian surface as seen from the Pathfinder landing site with the description of variations in the vertical height of the Martian atmosphere for a given longitude and latitude values, $Z_{(l,l)}$. Bottom right is the description of the slant height, s, and the zenith angle, θ, used in the calculations for the effective shielding from the atmosphere at a given target point on the Martian surface.

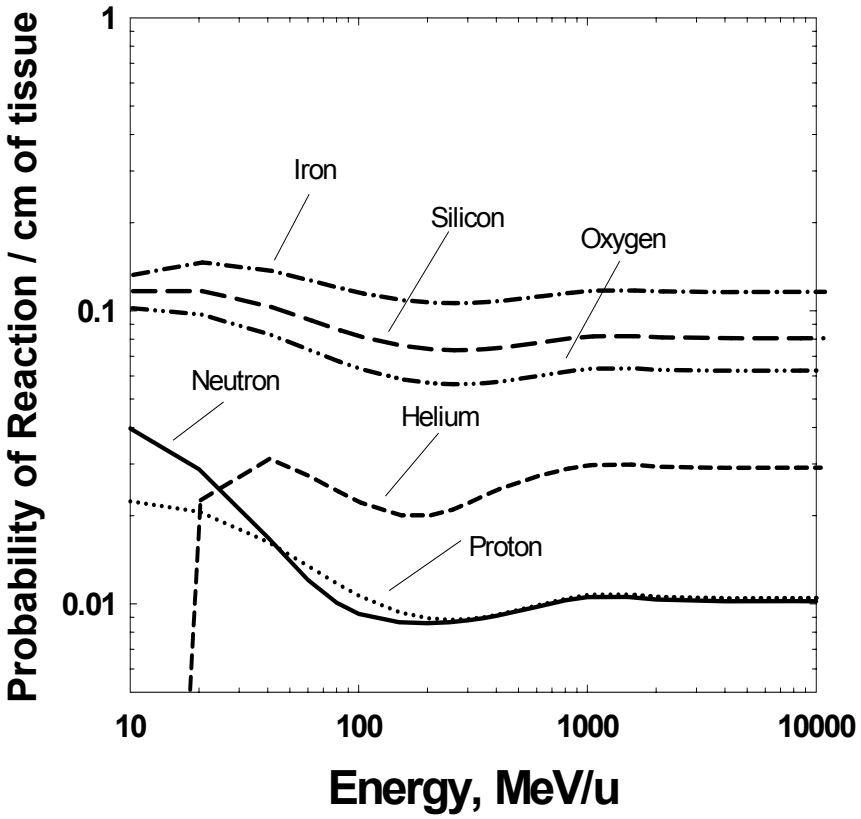

Fig. 2a. The probability of a nuclear reaction per cm of tissue traversed versus energy for several ions prominent in the GCR.

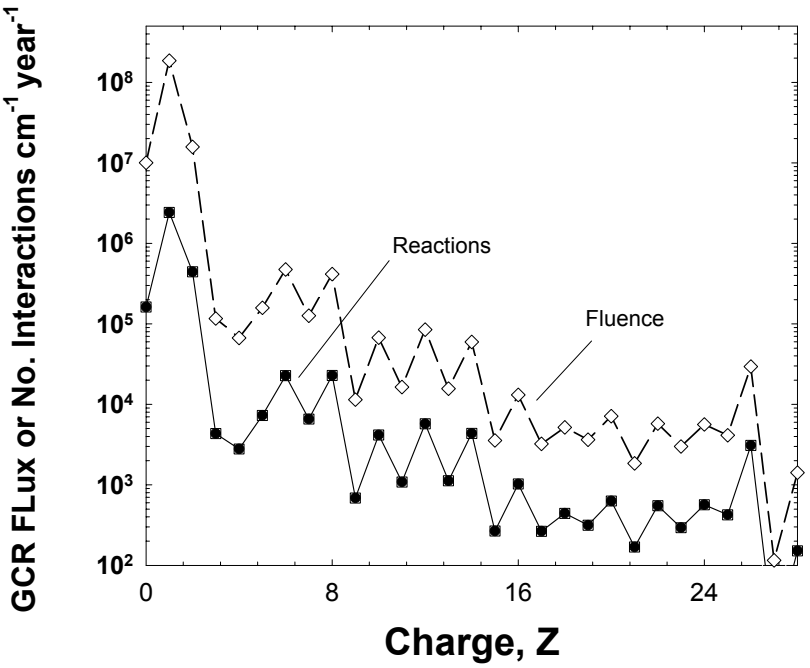

Fig. 2b. Comparisons of the elemental fluence of GCR ions near solar minimum to the number of nuclear interactions that occur per cm of tissue traversed by each charge GCR group. Calculations are made behind 5 cm of tissue.

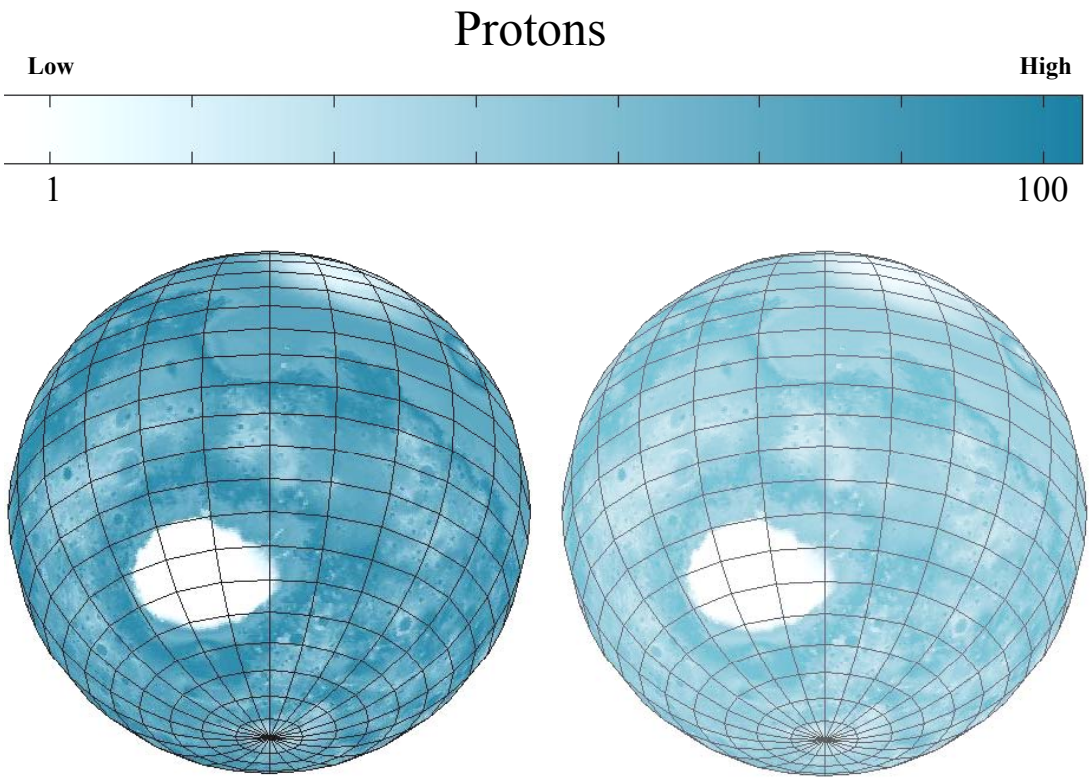

Figure-3. The number of proton hits per cell per year on the Martian surface. Calculations consider the transport of the GCR through the Mars atmosphere using the MOLA topographical data. These particle flux calculations consider the extreme solar cycle scenarios with calculations with left panel near solar minimum (with solar deceleration parameter, $\varphi = 428$ MV) and right panel solar maximum scenario ($\varphi = 1050$ MV) are shown. Estimates of proton hits per cell per year are for an average location on the skin including the self-shielding of the astronauts body.

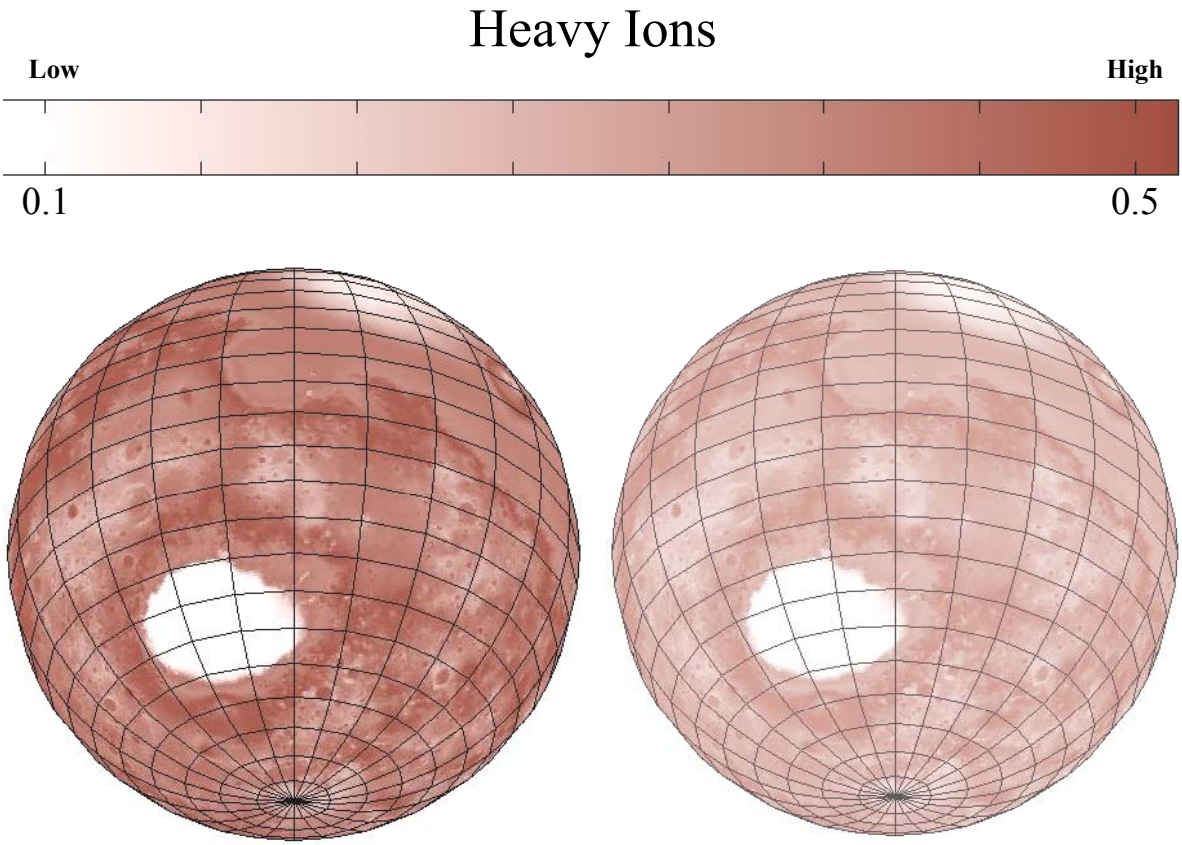

Figure-4 The number of heavy ion (Z>2) hits per cell per year on the Martian surface. Calculations consider the transport of the GCR through the Mars atmosphere using the MOLA topographical data. These particle flux calculations consider the extreme solar cycle scenarios with calculations with left panel near solar minimum (with solar deceleration parameter, φ = 428 MV) and right panel solar maximum scenario (φ = 1050 MV) are shown. Estimates of proton hits per cell per year are for an average location on the skin including the self-shielding of the astronauts body.

Figure-5. Comparison of calculated particle hits per cell per year at the skin on the Martian surface for solar minium and solar maximum conditions. Results for protons, alpha, light, medium, and heavy charge groups are shown

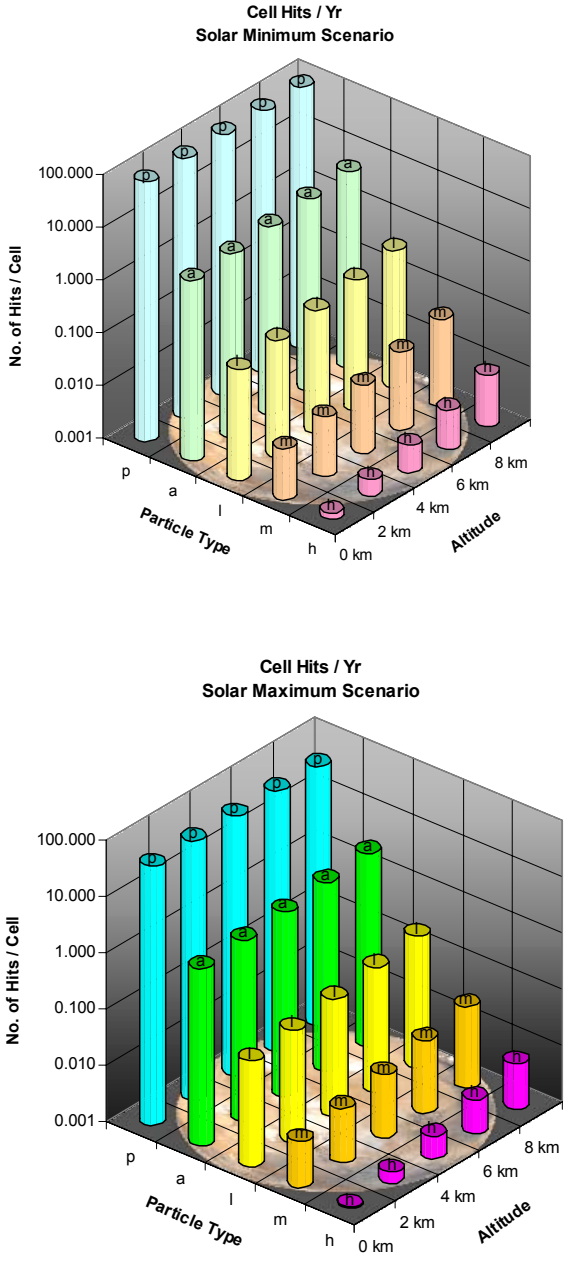

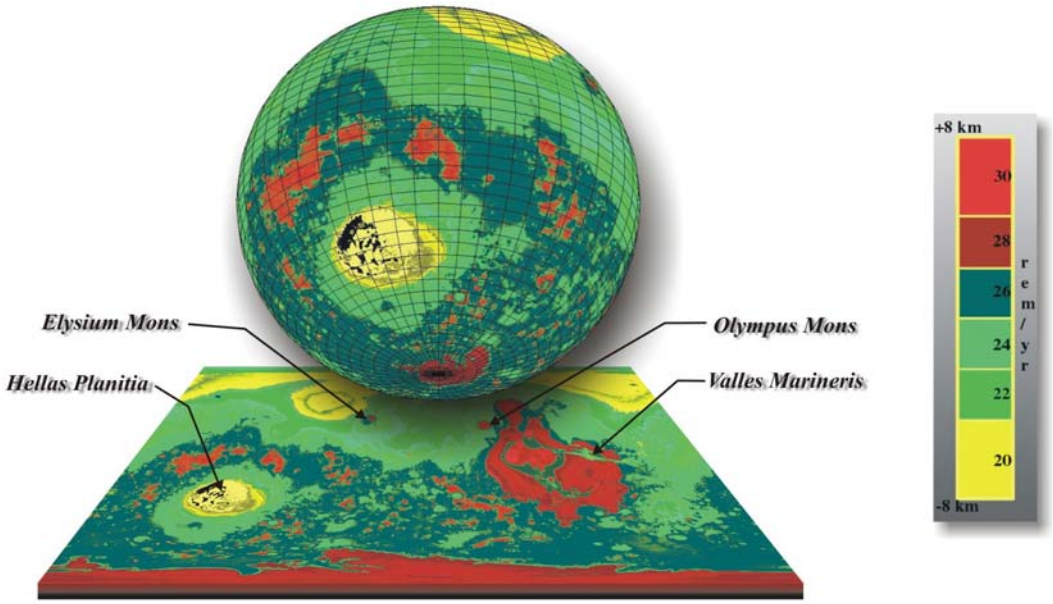

Figure-6. Calculations of the skin dose equivalent for astronauts on the surface of Mars near solar minimum. The variation in the dose with respect to altitude is shown. Higher altitudes (such as Olympus Mons) offer less shielding from the CO_2 atmosphere and lower altitudes (such as Hellas Planatia). The effective total dose has a range between 20 and 30 cSv/yr as a function of altitude for the static atmospheric model used here.